The Role of Planetary Waves in the Downward Influence of Stratospheric Final Warming Events

LANTAO SUN

Department of Earth and Atmospheric Sciences, Cornell University, Ithaca, New York

WALTER A. ROBINSON

Department of Marine, Earth, and Atmospheric Sciences, North Carolina State University, Raleigh, North Carolina

GANG CHEN

Department of Earth and Atmospheric Sciences, Cornell University, Ithaca, New York

(Manuscript received 4 January 2011, in final form 6 April 2011)

ABSTRACT

Stratospheric final warming events are simulated in an idealized atmospheric model by imposing a winter-to-summer transition in radiative equilibrium temperature only in the stratosphere. Large ensembles of events are simulated with different strengths of topographic forcing. It is found that the dates of final warmings become earlier and their downward influence on the troposphere becomes stronger for greater topographic amplitudes. This result is similar to observed differences between the downward influence of the final warming in the Northern and Southern Hemispheres. The mechanisms through which the final warming exerts its influence on the tropospheric circulation are investigated using a zonally symmetric model. It is found that lower-stratospheric wave driving induces a residual circulation that affects the tropospheric circulation. The stratosphere also affects the propagation of planetary waves in the upper troposphere, resulting in a burst of wave activity and a rapid deceleration of tropospheric zonal winds at the time of the final warming. These results highlight the important roles of planetary waves in the downward influence of the stratospheric final warming events.

1. Introduction

The stratosphere undergoes a final collapse of the polar vortex, appearing as a polar warming and the reversal of zonal winds from wintertime westerlies to summertime easterlies, in the spring as solar heating in high latitudes increases (Andrews et al. 1987). This so-called stratospheric final warming differs from the sudden warming in that the final warming occurs every year in both hemispheres. Also, unlike the sudden warming, the easterly zonal winds after the final warming do not return to westerly until the final cooling takes place during the fall. The date on which the polar vortex breaks up, the so-called final warming onset time, varies from year to year. The interannual variability in the timing of the final warmings depends on the strength of planetary wave forcing (Farrara and Mechoso 1986), and it can have a large impact on the chemical depletion of stratospheric ozone (Salby and Callaghan 2007). A late final warming is often associated with more ozone loss, because there is less ozone transport from the midlatitudes and increased chemical destruction within the polar vortex. For example, Waugh and Rong (2002) found there are large differences in the mixing of Arctic vortex air into the midlatitudes between early and late final warmings.

Recent observational analyses connected the stratospheric final warming to the seasonal transition in the troposphere. Black et al. (2006, hereafter BMR06) and Black and McDaniel (2007b, hereafter BM07b) constructed zonal wind composites for the final warming in both hemispheres. The Northern Hemisphere (NH) has a coherent pattern of significant zonal wind anomalies (defined as deviations from the climatological seasonal cycle) in the high-latitude stratosphere extending downward

Corresponding author address: Lantao Sun, Department of Earth and Atmospheric Sciences, Cornell University, Ithaca, NY 14850.
E-mail: ls544@cornell.edu

DOI: 10.1175/JAS-D-11-014.1

to the surface. In the Southern Hemisphere (SH), however, only marginally significant anomalies are observed in the troposphere. Monthly analyses of final warmings by Ayarzagüena and Serrano (2009) also revealed that the NH final warming has a substantial impact on the tropospheric storm tracks over the North Atlantic and the numbers of storms that cross northern Europe during April. In an idealized atmospheric dynamical model, Sun and Robinson (2009) simulated final warming events by imposing a transition in radiative equilibrium temperature from winter to summer only in the stratosphere. Their ensembles of final warming results with and without topography showed that a substantial fraction of the observed tropospheric changes that occur in conjunction with final warmings are induced from the stratosphere. These observational analyses and model results all suggest that the stratospheric final warming can make a significant contribution to the springtime transition in the lower troposphere.

In support of observations of the downward influence from the stratosphere, several possible mechanisms have been proposed to explain how the stratosphere can affect the tropospheric circulation. Persistent wave driving in the stratosphere induces a secondary circulation that transmits the stratospheric signal downward to the surface (Haynes et al. 1991). This ''downward control'' result is the equilibrated response to stratospheric forcing. The short-term tropospheric response, on the other hand, can be obtained by inverting rapidly evolving stratospheric potential vorticity (PV) anomalies, or the PV tendency (e.g., Black 2002). In a zonally symmetric model, Thompson et al. (2006) studied the zonal-mean balanced response to the stratospheric wave driving and found it was quantitatively similar to the observed tropospheric response to stratospheric vacillation.

Alternative mechanisms emphasize the role of tropospheric synoptic eddies in amplifying the signals originating in the stratosphere (Robinson 1994, 1996, 2000; Kushner and Polvani 2004). In observations and in model simulations, Chen and Held (2007) and Chen and Zurita-Gotor (2008) found that the stratospheric anomaly could modify the zonal propagation of tropospheric eddies and thus affect the tropospheric eddy momentum flux. This mechanism could explain the recent poleward shift of the SH surface westerlies during recent decades.

Song and Robinson (2004, hereafter SR04) tested the hypothetical mechanism of ''downward control with eddy feedback,'' which involves the tropospheric eddy reinforcement of a weak signal transmitted downward from the stratosphere by the residual circulation. Their experiments indicate that, in addition to these two mechanisms, planetary waves transmit a significant portion of the dynamical signal from the stratosphere to the troposphere, even when these waves are weak. Since planetary waves propagate upward from the troposphere to the stratosphere, stratospheric influence on planetary waves could include trapping of the waves near the tropopause (Chen and Robinson 1992) and wave reflection (Perlwitz and Harnik 2003, 2004). Recent studies by Black and McDaniel (2007a, hereafter BM07a) reveal that in the NH, the stratosphere can affect the tropospheric circulation directly prior to the final warming, and that after the final warming onset it can still affect the troposphere by vertically trapping the tropospheric waves.

Gerber and Vallis (2007) found that the intrinsic time scale of the annular mode is shorter in the presence of topography or other stationary wave forcing. This implies a weaker transient eddy feedback when the jet is not zonally symmetric. As a transient event, it is possible that the final warming does not allow enough time for the synoptic eddies to respond systematically, so that the tropospheric eddy feedback in the presence of topography will be weaker than its absence (e.g., SR04). On the other hand, SR04 suggested that the importance of planetary waves in coupling the troposphere to the stratosphere would increase in the presence of realistic planetary waves. This suggests that in final warming simulations, when the topographic forcing is strong enough, the influence of planetary waves on the troposphere may exceed that of synoptic eddies; the modeling results that we report on here support this suggestion.

This paper contains five sections. Section 2 provides a short description of the idealized dynamical model, the simulation, and how the results are diagnosed. Section 3 reports the results of ensembles of simulated final warmings with different topographic amplitudes. In section 4, we discuss the dynamics of the final warmings, focusing on the mechanisms of the downward influence. Section 5 presents conclusions. The dynamical model and zonally symmetric model are briefly described in the appendixes.

2. Models and diagnoses

a. Model and simulations

The idealized dynamical model is a primitive equation, hydrostatic, spectral model derived from the 1990s version of the Geophysical Fluid Dynamics Laboratory (GFDL) atmospheric model (Gordon and Stern 1982). The model has a dry atmosphere and radiative processes are represented by the Newtonian cooling parameterization. The same model has been used by SR04 to study the mechanisms for the stratospheric influences on the troposphere. For our studies we have made some changes to the equilibrium temperature and to the Newtonian cooling rate.

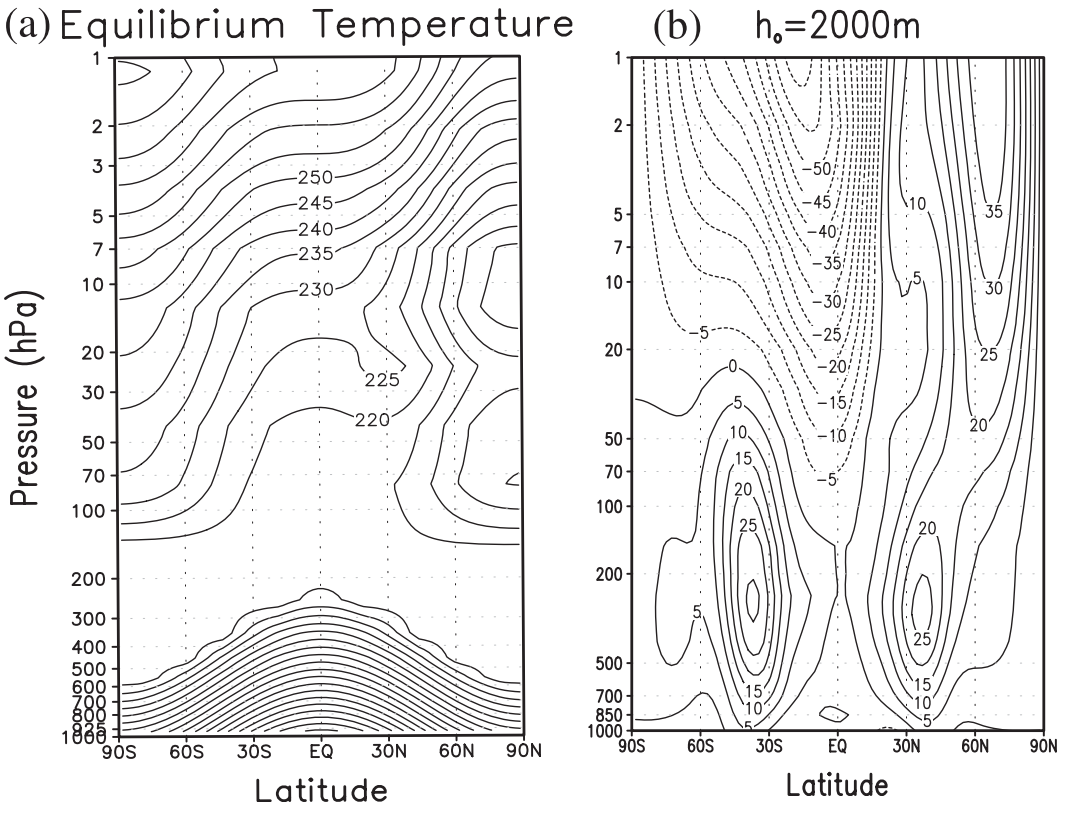

FIG. 1. (a) Radiative equilibrium temperature used in the perpetual run. The NH and SH are in the midwinter and midsummer, respectively. The contour interval is 5 K. (b) Climatological zonal wind in the perpetual run by fixing the equilibrium temperature as in (a) with 2000-m wave-1 topography in the NH. The contour interval is 5 m s^{-1}. The stratospheric radiative zonal wind is adopted from Scott and Haynes (1998) with slight changes. The tropospheric equilibrium temperature is from Held and Suarez (1994) (see appendix A for details).

The model is run at rhomboidal 30 (R30) spherical harmonic truncation (equivalent to 96 and 80 grid points in zonal and meridional directions). Rhomboidal 60 (R60) truncation is used in some simulations. Sigma coordinates are adopted in the vertical, where $\sigma = p/P_s$, p being the pressure and P_s the surface pressure. We use the same levels as Scinocca and Haynes (1998) and SR04. There are $n_F = 30$ "full" levels and $n_F - 1$ "half" levels. The model domain extends from the surface of the earth up to about 105 km. A detailed description of the model is given in appendix A.

The stratospheric final warming is the final collapse of the polar vortex due to increased solar heating as spring progresses. Therefore, a seasonal transition is needed to produce and analyze final warmings. In the dynamical model, radiative diabatic heating/cooling is parameterized by Newtonian cooling, which relaxes model temperatures toward the radiative equilibrium temperature T_{eq}. The seasonal cycle is induced by a radiative relaxation to a seasonally varying, zonally symmetric T_{eq} field, which is a sinusoidal transition between winter and summer equilibrium temperature fields (cf. Scott and Haynes 2002).

We first run the model with T_{eq} fixed for 2000 days in order to obtain statistically stable winter and summer states in the NH and SH, respectively. The next 800-day output is branched out every 10 days for the 365-day seasonal transition, with T_{eq} evolving according to

$$T_{eq}(\phi,\sigma,t) = \gamma(t) \times T_{eq}^{winter}(\phi,\sigma) + [1 - \gamma(t)] \times T_{eq}^{summer}(\phi,\sigma), \quad (1)$$

where $\gamma(t) = 0.5 \times [1 + \cos(2\pi \times t \text{ days}/365 \text{ days})]$ and $T_{eq}^{winter}(\phi,\sigma)$ and $T_{eq}^{summer}(\phi,\sigma)$ are the midwinter and midsummer T_{eq}, which are shown in Fig. 1a. This yields an 80-member ensemble of seasonal transitions. Because the winter and summer T_{eq} are the same in the troposphere, the seasonal transition is driven radiatively only in the stratosphere. This experimental design allows us to look at how the stratospheric final warming affects the tropospheric circulation.

To test the final warming under different topographic forcings, six different topographic amplitudes from 500 to 3000 m are applied to the seasonal runs. For the 2000-m

topography, we also test different stratospheric vortex strengths by setting the radiative polar stratospheric jet parameter u_1 (see appendix A) to 200, 240, 320, and 360 m s^{-1}, instead of the value of 280 m s^{-1} used in the control run. In addition, runs are carried out with wavenumber-2 topography and at higher resolution (R60) to examine the robustness of the results. Each seasonal transition comprises an 80-member ensemble.

b. Zonally symmetric model

We use a zonally symmetric model to evaluate the roles of different wave forcings in driving the downward influence during the final warming. The zonally symmetric model uses the same radiative forcing and dissipations as the full model, but only the zonally symmetric component (spectral zonal wavenumber 0) is integrated forward in time. Since the zonally symmetric model computes its own residual circulation in response to the wave driving, it can be used to evaluate the influence of the stratospheric wave driving on the circulation (e.g., Kushner and Polvani 2004; Thompson et al. 2006). In the zonally symmetric model, the eddy forcings are not internally generated. They must be imposed, and are diagnosed from the results of the full model. There is no topography in the zonally symmetric model. Note that the eddy forcing is calculated daily from the output of the full model, so it can be used to simulate transient events in the zonally symmetric model. A detailed description of the eddy forcings is given in appendix B.

c. Diagnostics

The dynamical model output includes daily spectral fields of vorticity, divergence, temperature, and surface pressure. When diagnosing the zonal mean and eddy terms, all of the calculations are performed within σ coordinates to avoid any inaccuracies. The zonal wind, meridional wind, temperature, and surface pressure are directly obtained from the spectral fields by fast Fourier transform (FFT); the other variables, such as σ vertical velocity $\dot{\sigma}$, potential temperature θ, and geopotential height Φ can be diagnosed in the same way as in the model. The transformed Eulerian mean (TEM) form of the momentum equation under σ and spherical coordinates is very similar to SR04 with slight simplifications. All the variables are then vertically interpolated from sigma coordinates to pressure coordinates for display.

3. Final warming results

a. Onset time

BMR06 and BM07b analyzed observations of the NH and SH final warmings using the National Centers for Environmental Prediction (NCEP)–National Center for Atmospheric Research (NCAR) reanalysis and 40-yr European Centre for Medium-Range Weather Forecasts (ECMWF) Re-Analysis (ERA-40) datasets. Here we adopt similar approaches to calculate the onset dates and to construct composites of final warmings. BMR06 define the onset date of the final warming as the final time that the zonal-mean zonal wind at 50 hPa and 70°N drops below zero without returning above a 5 m s^{-1} threshold. The latitude 70°N is chosen because it is the latitude of the NH stratospheric jet. Similarly, 60°S is used to define the final warming in the SH (BM07b). For our seasonal transitions, the final warming onset dates are based on the latitudes of the midwinter stratospheric jet in each run, increasing from 55° to 70°N with the amplitude of topographic forcing. In addition, when the topographic forcing is strong, the zonal wind variability during the seasonal transition is large, so that the 50-hPa zonal wind often exceeds 5 m s^{-1} even during the summertime. Thus we adopt a larger returning threshold, 10 m s^{-1}, in this study to avoid categorizing such events as very late final warmings. In the SH observations, because of the weakness of SH planetary waves, if defining the final warming as a change in sign of the zonal wind, final warmings do not always occur at 50 hPa. Therefore, BM07b adjust the definition transition threshold to 10 m s^{-1}. Here we use 20, 10, and 5 m s^{-1} transition thresholds to define the 50-hPa final warmings with 500-, 1000-, and 1500-m topography.

The left panel of Fig. 2a shows the 50-hPa ensemble-mean final warming onset dates for different topographic amplitudes, together with the observations for both hemispheres. Here the final warming onset dates are the number of days after the transition in the equilibrium temperature begins [t in Eq. (1) in the simulation] and the number of days after the winter solstice for the observations. The final warming onset dates become earlier as topographic amplitudes increase. The mean onset date for NH observational final warmings is close to the mean dates obtained in our model for 1500-m topographic amplitude, but since the transition threshold for the final warming with 1500-m topography is 5 m s^{-1}, the NH observational mean onset date should be between the 1500- and 2000-m cases. The date for SH is even later than our 500-m amplitude result.

The right panel of Fig. 2a shows the ensemble-mean onset dates of final warmings for different vortex strengths with the same 2000-m topographic forcing. For the same topographic forcing, the difference in onset time results from the different T_{eq} forcing in the spring transition. For a larger u_1, the radiative zonal wind in the stratosphere will also be larger during the spring transition so that the final warming occurs later.

The standard deviations for the onset dates are shown in Fig. 2b. The standard deviation always increases

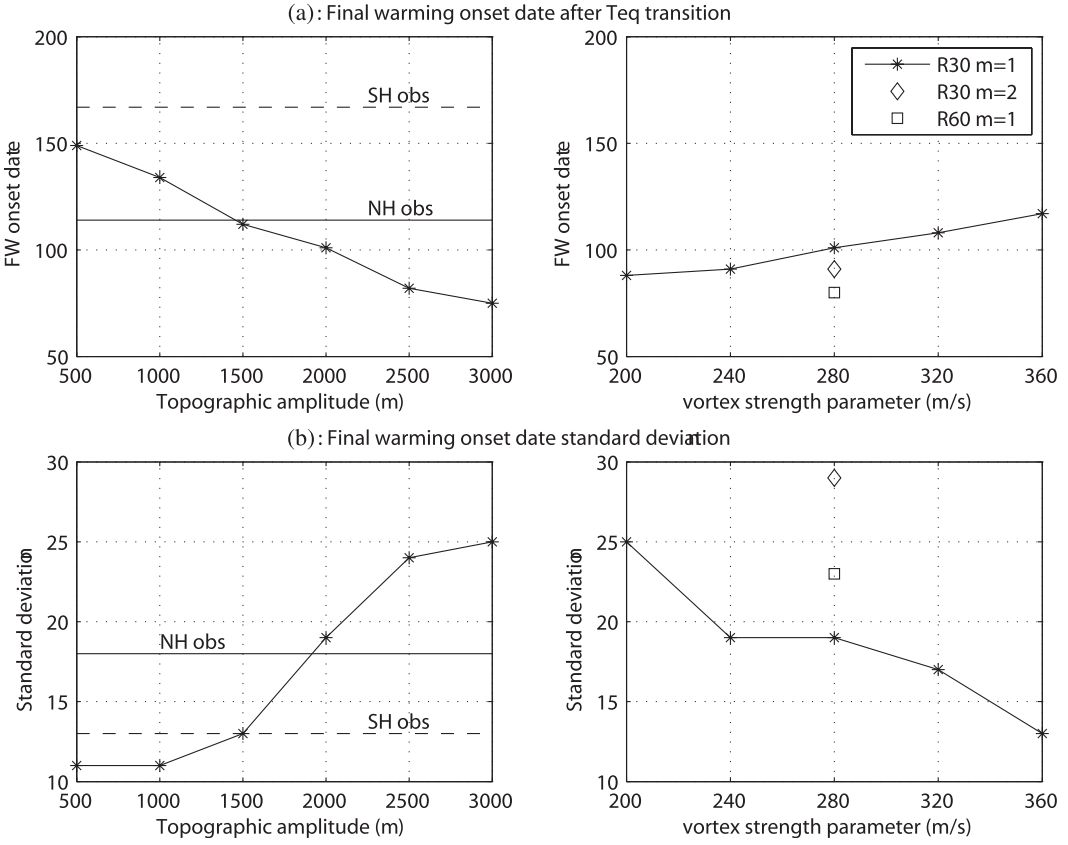

FIG. 2. The stratospheric final warming (a) 80-member ensemble mean onset dates and (b) standard deviations of the onset dates for different topographic forcing (h_0, m), vortex strength u_1, and horizontal resolutions. The onset date is the date after the transition of equilibrium temperature begins and is defined at 50 hPa (see the text for details). The NH mean onset date and standard deviation of the onset dates for the period 1958–2004 from the NCEP–NCAR reanalysis dataset are denoted as solid lines in the left panels (BMR06). The SH mean onset date and standard deviation of the onset dates for the period 1978–2001 from the ERA-40 dataset are plotted as dashed lines in the left panels (BM07b).

monotonically with the strength of the topographic forcing. For the different stratospheric vortex strengths, a large radiative zonal wind during the spring transition is associated with a late final warming and small variability in its timing, while a small radiative zonal wind during the spring transition is associated with early final warmings with more variable timing.

The dates of occurrence for the 50-hPa final warming events with different topographic amplitudes appear to be approximately normally distributed, as is the case for the observed NH final warmings (not shown). The observed distribution of final warming dates in the SH is more complicated, since it can include trends resulting from anthropogenic ozone depletion (BM07b).

b. Zonal wind evolution during the final warming

After the final warming onset dates are determined, ensemble composites are constructed by performing ensemble averages with the time axis for each ensemble member shifted to align the onset times. This is different from ensemble climatology, in which the time is based on the evolution of T_{eq}. Composite anomaly fields are calculated by subtracting the ensemble climatology from the ensemble composites. To estimate the statistical significance of the anomalies, the two-sided Student's t test is used to calculate the 95% confidence level.

Figure 3 shows the evolution of the zonal wind climatologies and composites at 50 hPa and 70°N across the final warmings for different topographic amplitudes. The 50-hPa level is used to define the final warming. From day −20 to day +20, the transition is characterized by the transition from westerlies prior to the final warming to easterlies afterward. When the topographic amplitude is weak (500-m amplitude), the zonal wind evolution is slow and there is little change over this 40-day period. For final warmings with 1000-m topography, the zonal wind deceleration is clear, but the composite and climatological evolutions overlap. For stronger topography, the abrupt

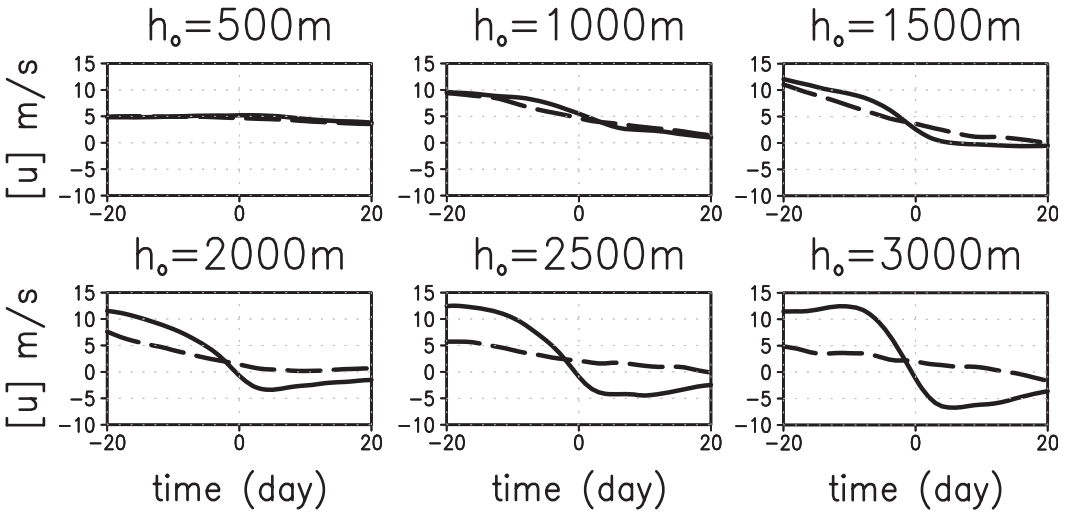

FIG. 3. Climatological (dashed) and composite (solid) zonal wind at 50 hPa and 70°N across the final warmings for different h_0 in the dynamical model. The abscissa denotes the day with respect to the final warming onset.

transition in the composite and the slower transition in the climatology are evident. For weaker planetary wave forcing, the transition is primarily driven by the seasonal cycle in radiative forcing, but as dynamical forcing becomes stronger, the warming becomes more dynamical, abrupt, and variable in timing. The latter leads to increasing differences between the climatological and composite evolution.

Similar features are present in the troposphere. Figure 4 shows the results for 200 hPa and 70°N. Once again, the differences between the climatology and the composite are small when the topographic forcing is weak. For topography stronger than 1000 m, the composite zonal wind deceleration appears before the final warming, while the climatological transition is much smaller.

Figures 3 and 4 characterize the high-latitude zonal wind transitions across the final warmings. Prior to the final warming, zonal winds decelerate not only in the stratosphere, but also in the troposphere. Such decelerations, however, are much slower in the stratospheric climatology and are not evident at all in the tropospheric climatology, from which they are filtered by averaging. The tropospheric zonal wind transitions in the composite are tied to the date of the stratospheric final warming.

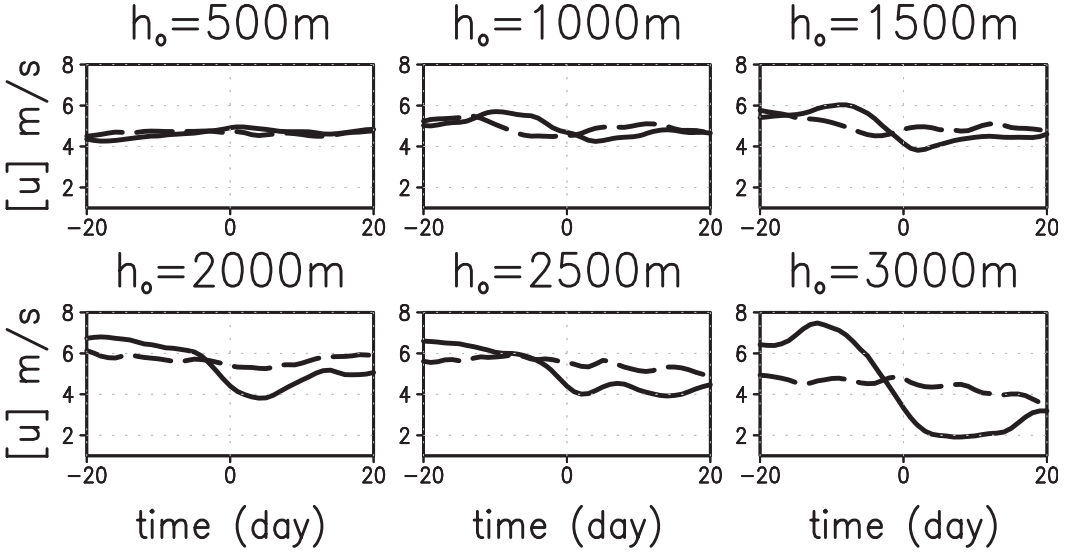

FIG. 4. As in Fig. 3, but at 200 hPa and 70°N.

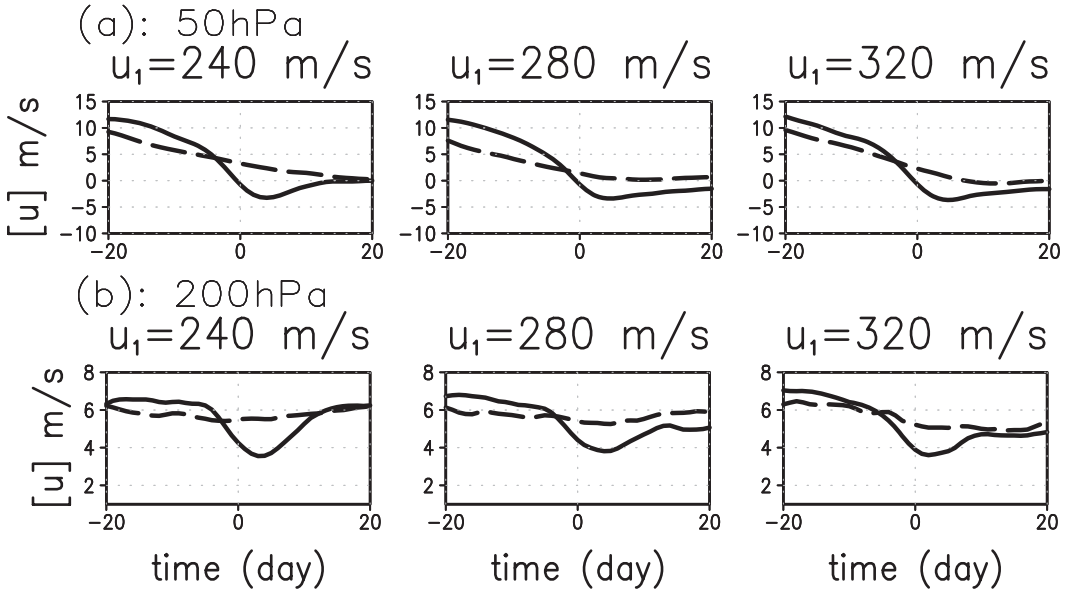

FIG. 5. Climatological (dashed) and composite (solid) zonal wind at (a) 50 and (b) 200 hPa and 70°N across the final warmings for different u_1 in the dynamical model. The abscissa denotes the day with respect to the final warming onset.

Since the final warming occurs in the stratosphere, we know that these tropospheric signals are initiated by stratospheric changes.

The zonal wind evolution with different vortex strengths for the standard (2000 m) topography is shown in Fig. 5. Although the onset times are different, the zonal wind transitions are similar in the stratosphere and the troposphere. Given that these three experiments have the same topographic forcing and similar equilibrium temperatures near the final warming onset, the zonal wind transitions in the stratosphere and troposphere should be similar.

c. *Robustness with respect to topographic wavenumber and resolution*

Ensembles of final warmings with wavenumber-2 topographic forcing and with higher resolution, rhomboidal 60 (R60) truncation, are used to test the robustness of our results. The mean onset date of final warmings for the wavenumber-2 topographic forcing is approximately 10 days earlier than for wavenumber-1 forcing (Fig. 2a, right). Since the midwinter polar vortex is similar in the perpetual runs using wave-2 and wave-1 topography, the earlier onset time of the wavenumber-2 final warmings implies that wavenumber 2 is more effective than wavenumber 1 in driving the zonal wind transition. Gerber and Polvani (2009) found that wavenumber 2 was more effective than wavenumber 1 in triggering sudden warmings in a similar idealized GCM. Our results are consistent with theirs.

We also run final warming ensembles with higher resolution. With higher resolution, more waves are resolved and the wave–mean flow interaction is stronger. This results in larger variability in the perpetual run (not shown) and an earlier date for the final warming onset. From Fig. 2a, the mean onset date for R60 with 2000-m topography is comparable to the results for 3000-m topography at R30 resolution.

The 50- and 200-hPa zonal wind evolutions across the final warmings are shown in Fig. 6. Although there are differences for different wavenumber forcings and different resolutions, the zonal wind decelerations in the composite are similar, confirming that the zonal wind transition in the stratospheric final warming and its impact on the troposphere are robust.

4. Dynamics of the final warming

In the previous section, we showed that the final warming can influence the tropospheric circulation when the topographic forcing is sufficiently strong. This influence is robust, as it appears with different wavenumbers for the topographic forcing and at different resolutions. The evolution of the zonal wind in final warmings with strong topographic forcing is more similar to the NH observations (BMR06) with regard to onset date and tropospheric response. In this section, we choose the 2000-m amplitude final warming as a strong topographic forcing event to study the dynamics of the final warmings, focusing on the mechanisms of the downward influence.

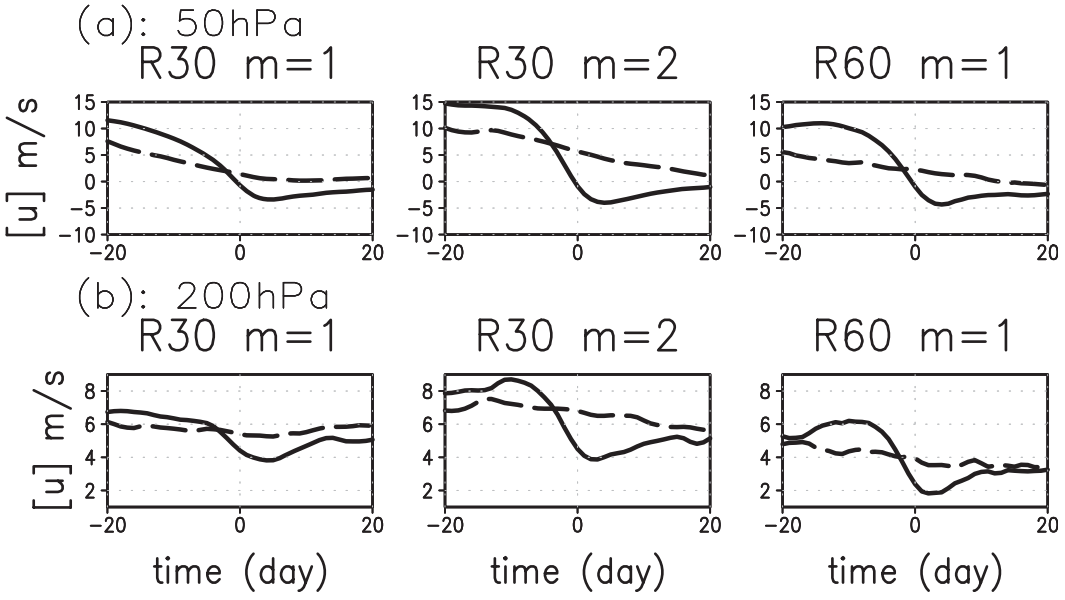

FIG. 6. Climatology (dashed) and composite (solid) zonal wind at (a) 50 and (b) 200 hPa and 70°N across the final warmings for different wavenumber topographic forcings and horizontal resolutions in the dynamical model. The abscissa denotes the day with respect to the final warming onset.

a. Final warming evolution

Since most of the zonal wind and wave anomalies are in high latitudes, we can summarize the evolution of the final warming by plotting the high-latitude behavior. The climatological and composite zonal winds, averaged over 65°–75°N, are shown in Fig. 7. The climatology is characterized by a slow transition from a winter state with westerlies to a quasi-steady summer state with easterlies in the stratosphere and a weak jet in the upper troposphere. There is very little change in the lower troposphere. In contrast, because our compositing procedure shifts the timing of each final warming to day 0, the composite zonal wind transition is much more abrupt in both the stratosphere and the troposphere. After the onset of the final warming, the composite zonal wind recovers slightly in the stratosphere because of the absence of planetary waves. The composite better reflects the typical evolution of the zonal wind because it avoids averaging over events that occur at different times.

The zonal wind anomalies in Fig. 8 show statistically significant positive anomalies prior to the final warming and negative anomalies afterward, implying a larger zonal wind deceleration in the composite than in the climatology. The negative anomalies extend coherently downward to the surface. The zonal wind changes are closely connected to the wave activity, as shown from the long wave Eliassen–Palm (E–P) flux vector and divergence. The transition of the zonal wind anomalies from positive to negative is accompanied by upward anomalous upward E–P flux vectors, and a large anomaly in the E–P flux convergence occurs prior to the final warming event. The zonal wind and wave evolutions in our simulation are similar to NH observations (BMR06).

b. The roles of planetary waves in the final warmings

Tropospheric synoptic eddies are important in amplifying the signals transmitted from the stratosphere (e.g., Kushner and Polvani 2004; SR04). Without topography, SR04 (see Fig. 10 of their paper) found that short waves are primarily responsible for the tropospheric response to stratospheric wave driving, although the influence of planetary waves is not negligible. Most of the planetary wave driving, in their model, is associated with wavenumber 3. In this study, wavenumber-1 topographic forcing is added to the model and the situation is different.

We estimate the roles of planetary waves by separating the longwave (numbers 1–3) from shortwave E–P flux. Figure 9 shows the comparison of the anomalous E–P flux vector and divergence averaged over days −5 to 0 for the long and short waves. During this stage, zonal wind decelerations occur in the stratosphere and troposphere. The upward E–P flux and E–P convergence in the extratropical stratosphere are responsible for the stratospheric deceleration. In the troposphere, there is a vertically oriented dipole in wave driving centered around 70°N with convergence above 700 hPa and divergence below. The E–P pattern for the long waves is similar to the wavenumber-3 structure shown in Fig. 11 of SR04. The

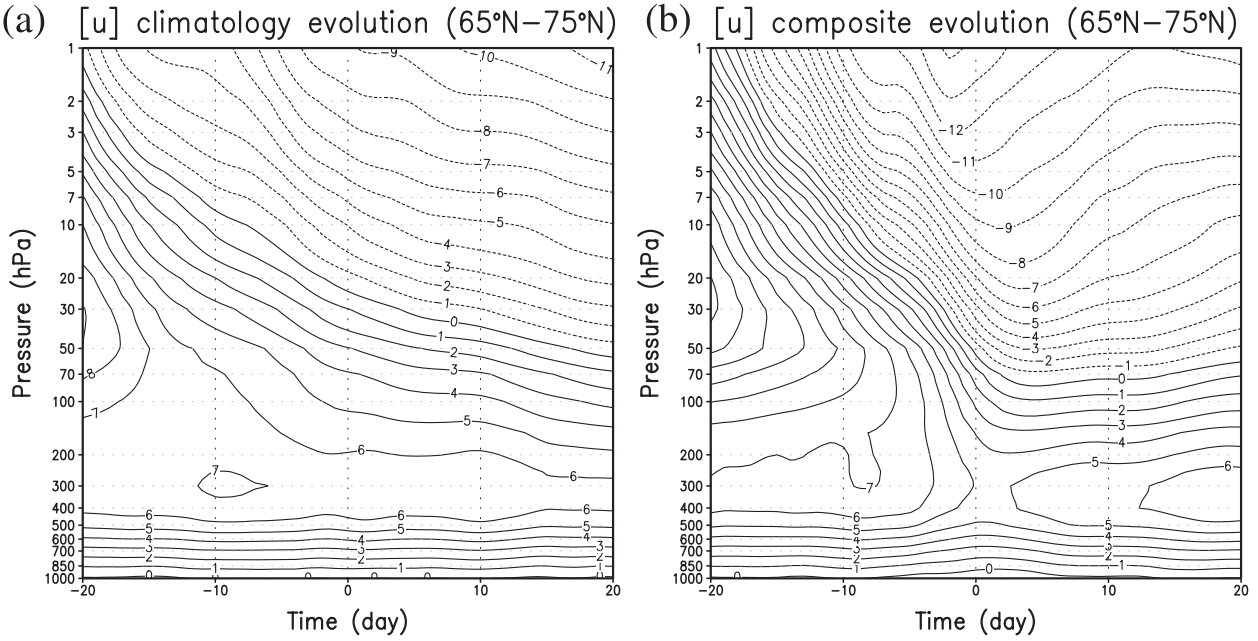

FIG. 7. (a) Climatological and (b) composite zonal wind averaged over 65°–75°N for the 2000-m topographic final warming events. The contour interval is 1 m s^{-1}. The abscissa denotes the day with respect to the final warming onset.

short waves, however, are largely confined to the midlatitudes and the magnitude of their wave driving is small compared with that of the long waves, even in the troposphere. This implies that the long waves are the primary source of the zonal wind decelerations, not only in the stratosphere but also in the troposphere. It suggests that the downward influence of the final warming is a process that involves interactions between long waves

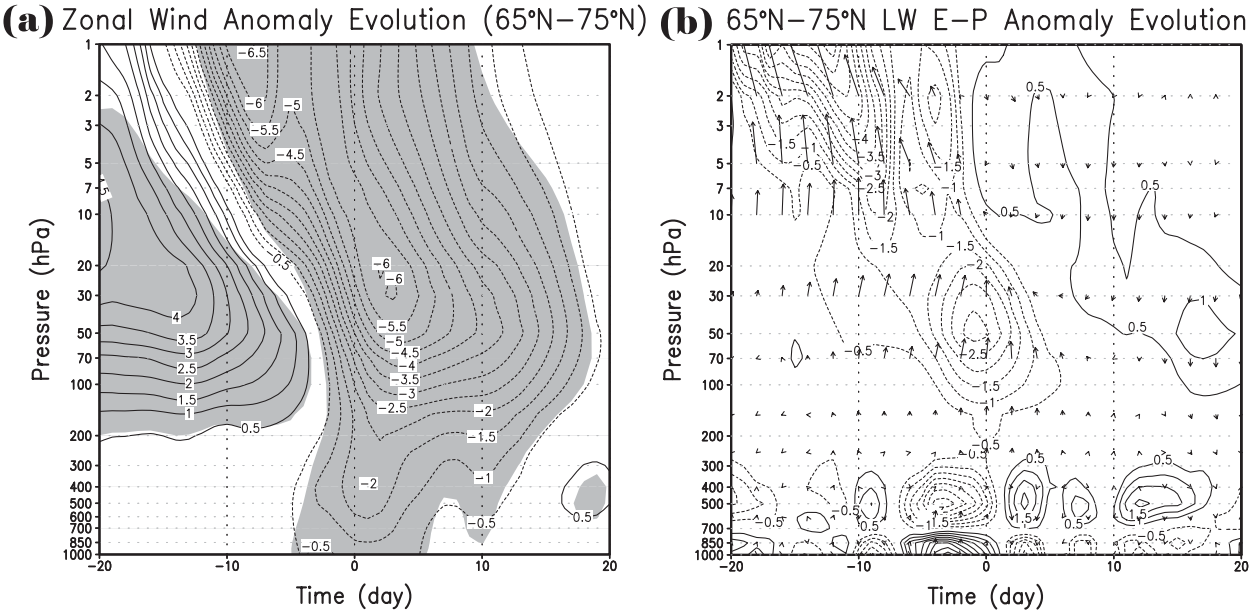

FIG. 8. (a) Composite anomalous zonal wind averaged over 65°–75°N for the 2000-m topographic final warming events. Gray shading denotes confidence levels of more than 95% that the anomalies are different from zero. The contour interval is 0.5 m s^{-1}. (b) As in (a), but for the anomalous longwave (numbers 1–3) E–P vector and E–P divergence. The E–P vector is plotted by $[F^{(\phi)}/\cos\phi, F^{(\sigma)} \times (10^9/P)]$, where F^{ϕ} and F^{σ} are horizontal and vertical E–P fluxes and P is the pressure level. The E–P divergence is plotted by the contours. The contour interval is 0.5 m s^{-1} day^{-1}. The abscissa denotes the day with respect to the final warming onset.

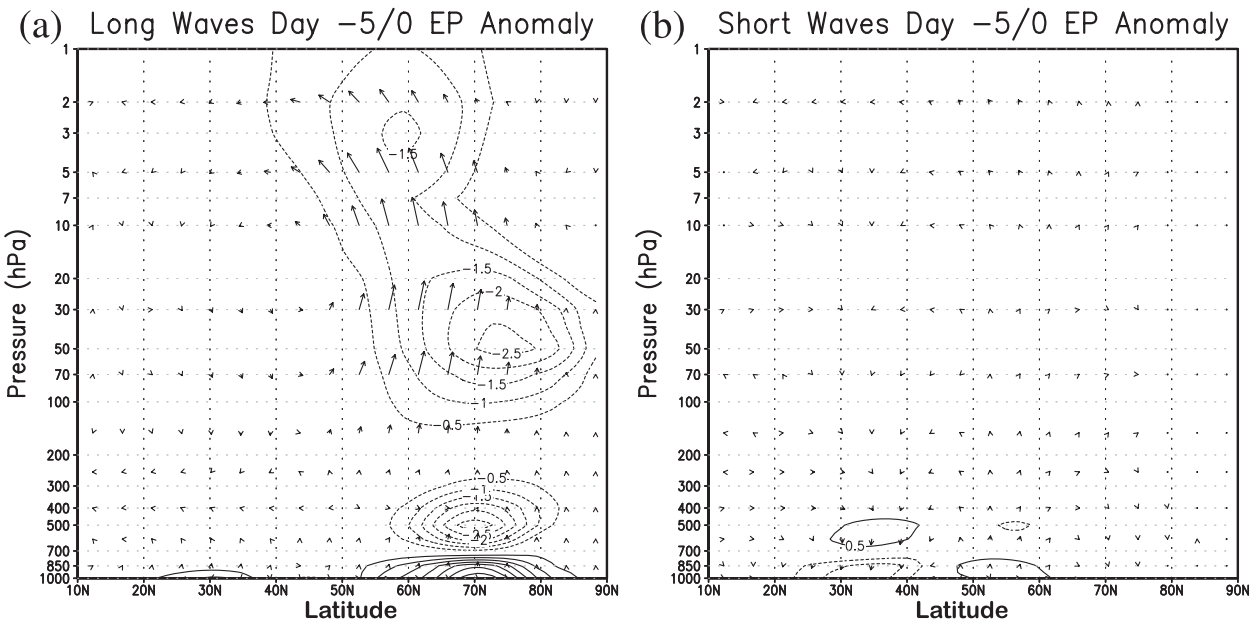

FIG. 9. (a) Anomalous longwave (numbers 1–3) E–P flux vector and E–P divergence averaged over days −5 to 0. The E–P flux vector is plotted as vectors, and E–P divergence is plotted by the contours. The contour interval is 0.5 m s^{-1} day^{-1}. (b) As in (a), but for the short waves (number > 3). The vector scale is identical to Fig. 8b.

and the zonal mean flow in the high latitudes where the tropospheric synoptic-eddy feedback is not important.

c. *Momentum budget analysis*

An analysis of the momentum budget can help to determine the roles of different terms in driving the zonal wind deceleration prior to the final warming, and so to understand better the mechanisms for the downward influence of final warmings. We use the σ coordinate TEM momentum equation (SR04), without considering the $\overline{(P_s' u')}_t$ term but including the near-surface drag,

$$\underbrace{\overline{P}_s \frac{\partial \overline{u}}{\partial t}}_{\text{Tendency}} = \underbrace{-\alpha \overline{v}^* - \beta \overline{\omega}^*}_{\text{Circulation}} \underbrace{- \frac{1}{\cos\phi} \left\{ \overbrace{\frac{1}{a\cos\phi} \frac{\partial [F^{(\phi)}]}{\partial \phi}}^{\text{Horizontal}} + \overbrace{\frac{\partial [F^{(\sigma)}]}{\partial \sigma}}^{\text{Vertical}} + \overbrace{\frac{1}{a} \overline{P_s' \frac{\partial \Psi'}{\partial \lambda}}}^{\text{Extra term}} \right\}}_{\text{E-P divergence}} \underbrace{- k\overline{u}}_{\text{Friction}}, \tag{2}$$

where $\overline{P}_s$ is zonal mean surface pressure; residual velocity is $(\overline{v}^*, \overline{\omega}^*)$; $\alpha = (1/a\cos\phi)[\partial(\overline{u}\cos\phi)/\partial\phi] - 2\Omega\sin\phi$; $\beta = \overline{u}_\sigma$; $\Psi = \Phi - RT$, where Φ is geopotential height; and $F^{(\phi)}$ and $F^{(\sigma)}$ are the horizontal and vertical E–P flux. In σ coordinates, there is an extra term on the right-hand side of the equation that cannot be explained as the divergence of a flux. Detailed information can be found in the appendix of Sun (2010). For the residual circulation term, the $\overline{\omega}^*$ term is found to be much smaller than the $\overline{v}^*$ term. From this equation, the stratosphere can affect the tropospheric circulation in two possible ways:

1) By changing the tropospheric residual circulation: this is the tropospheric geostrophic and hydrostatic adjustment to the stratospheric wave driving, such as the downward control theory (Haynes et al. 1991). When the stratosphere experiences the seasonal transition, it causes changes in the tropospheric residual circulation, which then affect the tropospheric zonal winds.
2) By changing the tropospheric waves: the stratosphere can affect the tropospheric planetary wave propagation by wave reflection (Perlwitz and Harnik 2003, 2004), wave refraction (Simpson et al. 2009), wave trapping (Chen and Robinson 1992; BM07a), or resonance (Scott and Haynes 2002).

We carry out the TEM momentum budget analysis for the perpetual winter and seasonal transition. In the

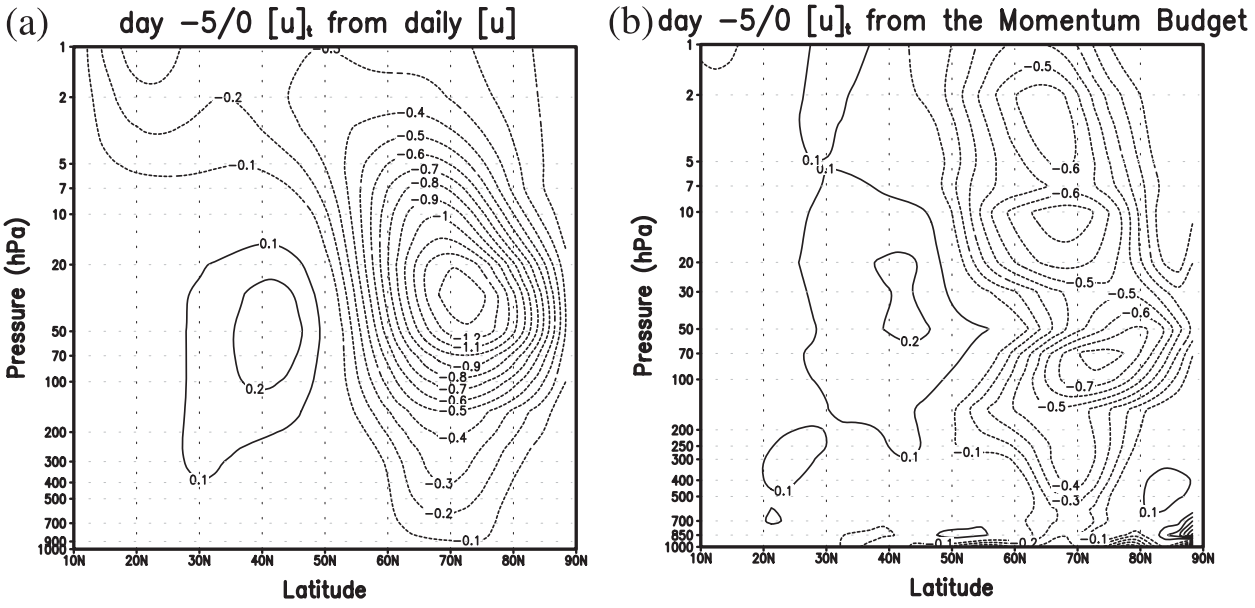

FIG. 10. (a) Anomalous zonal wind tendency averaged over days −5 to 0 calculated from daily zonal wind output. (b) As in (a), but calculated from the momentum budget. The contour interval is 0.1 m s^{-1} day^{-1}.

long-term mean perpetual winter state, there is a rough balance among the residual circulation, waves, and friction, and the zonal-wind tendency term is negligible. The zonal-wind tendency cannot be neglected in the final warming, however. There are two ways to calculate it: either directly from the daily zonal wind output or indirectly from other terms in the momentum equation. Here we use both methods to compute the climatological and composite zonal wind tendency for the 80-member final warming ensemble.

Figure 10 shows the anomalous zonal wind tendency averaged over days −5 to 0 calculated separately from the daily zonal wind output and from the momentum equation. The high-latitude deceleration is very clear in both, except in the upper stratosphere. Overall, there is a good agreement in the lower stratosphere and troposphere. There are more small-scale structures in the zonal wind tendency obtained from the momentum budget than from daily output. This is reasonable since the tendency from the daily output is a small residual from the sum of several large terms.

We then focus on the momentum budget and investigate which terms are responsible for the deceleration. Figure 11 shows the composite anomalies, averaged over days −5 to 0, of the residual circulation, E–P flux divergence, friction, and zonal wind tendency. The latter is obtained by combining the previous three terms. The friction is found to be negligible, except near the surface, where it acts against the zonal wind tendency, and is still much smaller than the E–P divergence and residual circulation terms. In the high latitudes of the stratosphere, most of the deceleration is caused by the E–P flux convergence, partly cancelled by the residual circulation. In the troposphere, the E–P flux convergence has nearly the same magnitude as the residual circulation so that the zonal wind deceleration is much smaller than in the stratosphere, and it only appears in the latitudes near 70°N.

The momentum budget for the final warming provides an estimate of the roles of the residual circulation, wave driving, and friction. In the stratosphere, the deceleration is mainly due to the E–P flux convergence, partly cancelled by the residual circulation. In the troposphere, wave driving is still important, and it has about the same magnitude as the residual circulation. Since there are both wave driving and circulation anomalies in the troposphere, it is not clear which mechanism dominates the downward influence. In fact, some portion of the residual circulation results from the local wave driving. Thus, from analyzing the momentum budget we cannot say if changes in wave driving or in the residual circulation, or in both, are induced by the stratospheric transition.

d. Zonally symmetric model results

Our zonally symmetric model allows us to compute separately the response to wave driving in different regions (stratosphere or troposphere) or due to different wavenumbers (long waves and short waves). Thus it can help to clarify the roles of different waves in contributing to the downward influence in our simulations (Fig. 8a).

The final warming run in the zonally symmetric model is carried out only for the composite and climatology rather than for each member of the ensembles. The initial

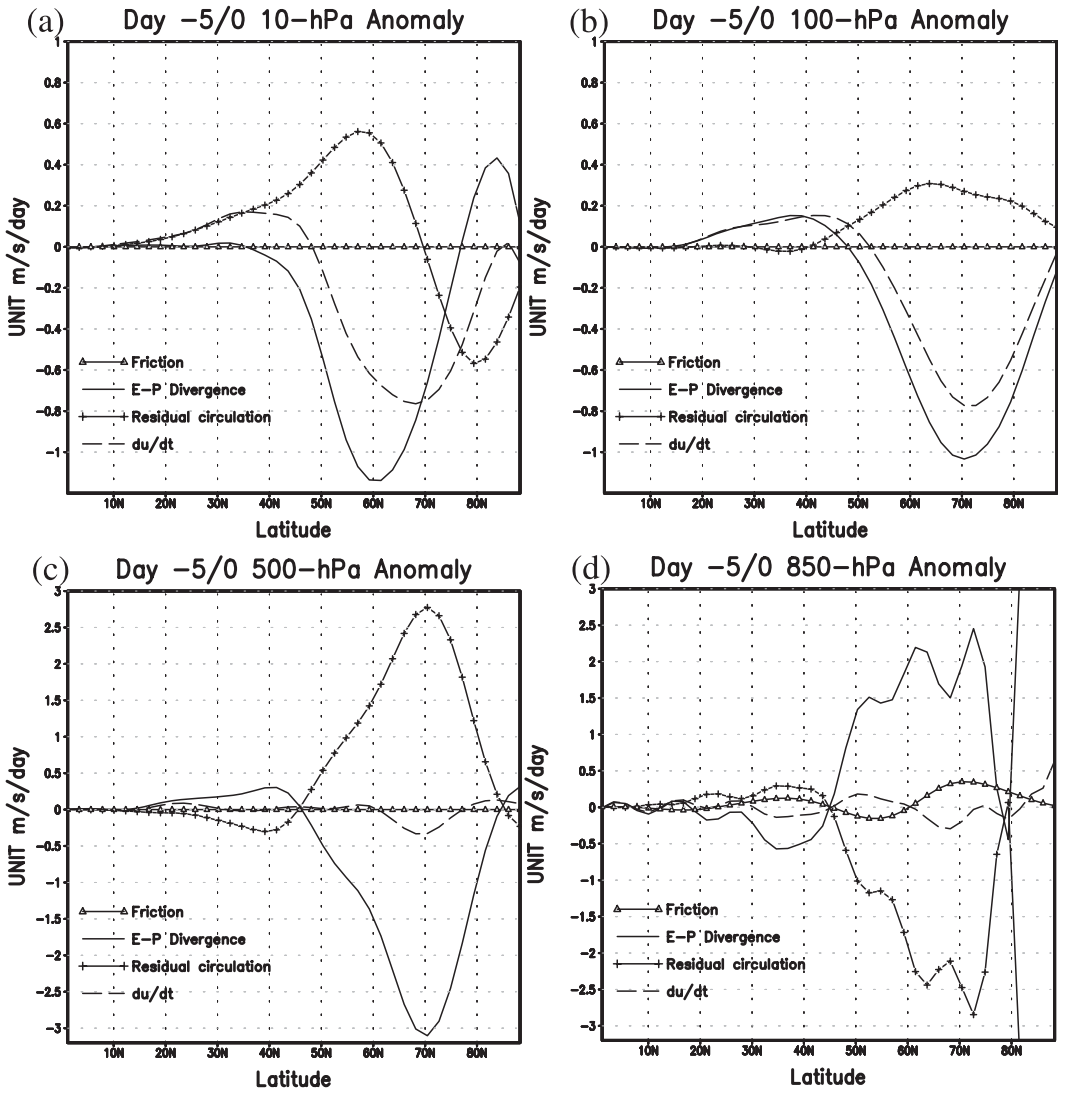

FIG. 11. Anomalous residual circulation (plus signs), E–P divergence (solid), friction (triangles), and zonal wind trend (dashed, calculated by adding the previous three terms) averaged over days −5 to 0 at (a) 10, (b) 100, (c) 500, and (d) 850 hPa. The unit is m s^{-1} day^{-1}.

conditions and eddy forcings are taken from the ensemble-mean composite and climatological final warming. Each run starts at day −40 with respect to the final warming onset and ends at day +40. The wave driving terms F_u, F_T, and $F_{\ln P_s}$ are updated daily. We first test the zonally symmetric model results by adding the total wave forcing diagnosed from the full model ensembles. The zonal wind anomaly evolution (not shown) is very similar to the results from the full models, indicating that full downward influence can be obtained in the zonally symmetric model when all of the wave driving is included.

We then separate the wave forcing into longwave ($m = 1 - 3$) and shortwave ($m > 3$) components. For each component, composite and climatology final warming runs are carried out. The anomaly evolutions across the final warming for the long and short wave forcings are shown in Figs. 12a,b. The evolution due to longwave forcing (Fig. 12a) closely resembles the ensemble mean from the full model. The evolution driven by shortwave forcing (Fig. 12b), however, is characterized by the weakening of the positive anomaly that was in the initial conditions. This result is very similar to that obtained without any wave forcing. This confirms the result, from section 4b, that the downward influence of the final warming in our model is associated with the long waves, and that synoptic-eddy feedback is not important. While the anomalous longwave forcing explains almost all of the anomalous evolution of the zonal wind (cf. Figs. 8a and 12a), the shortwave forcing is still important in maintaining the climatological flow in the troposphere.

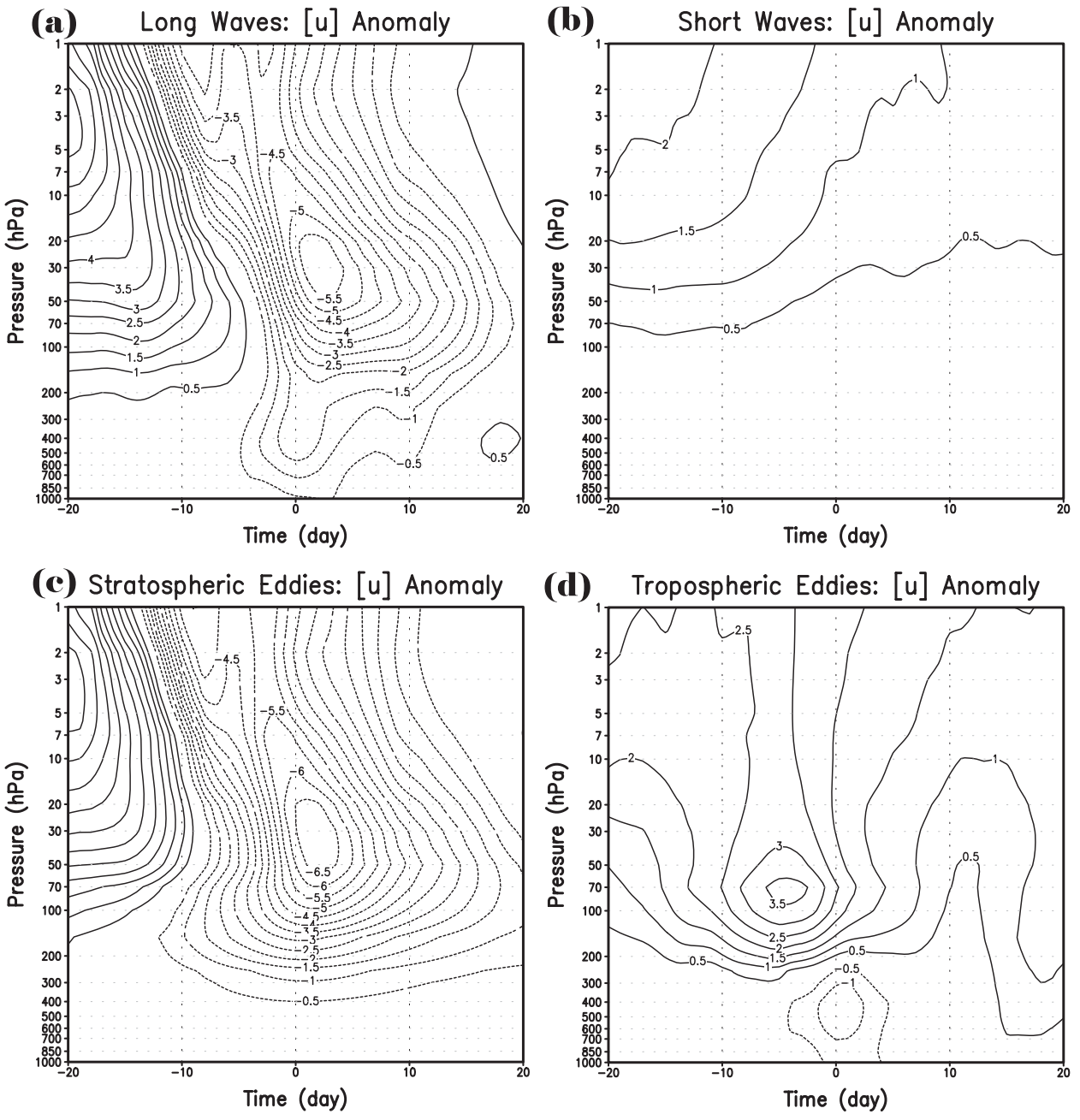

FIG. 12. (a) Composite anomalous zonal wind averaged over 65°–75°N across the final warming in the zonally symmetric model with only longwave ($m = 1$–3) forcing. The abscissa denotes the day with respect to the final warming onset. (b)–(d) As in (a), but only with (b) shortwave ($m > 3$), (c) stratospheric wave, and (d) tropospheric wave forcing. In the zonally symmetric model, climatological and composite eddy forcings are constructed from the full model 80-member ensemble final warmings with 2000-m topographic amplitude, as are the initial conditions. Anomaly evolution is computed by subtracting the climatology from the composite. Stratospheric and tropospheric eddy forcings are separated at 100 hPa.

The similarity between the anomaly fields means only that short waves are not important in driving differences between the composite and climatology.

Next, wave driving is separated into stratospheric and tropospheric components, using a boundary at 100 hPa. The results for the anomalous zonal wind are shown in Figs. 12c,d. In the stratosphere, the evolution with stratospheric forcing is similar to the full-model ensemble mean shown in Fig. 8. Anomalous zonal winds appear in the upper troposphere, but not in the lower troposphere. In

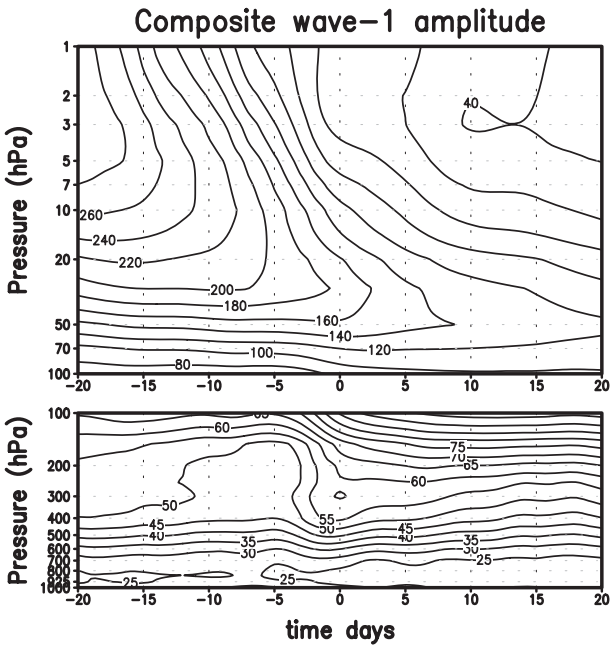

FIG. 13. Composite wave-1 amplitude averaged over 65°–75°N across the final warming in the full model. The contour interval is 5 m below 100 hPa and 20 m above 100 hPa. The abscissa denotes the day with respect to the final warming onset.

contrast, the evolution of the anomalous zonal wind with tropospheric forcing shows negative anomalies in the lower troposphere near the onset of the final warming. When wave driving at levels between 100 and 250 hPa is included in the stratospheric component, the downward influence due to stratospheric forcing extends into the lower troposphere. Wave driving down to levels below 500 hPa, however, must be included to obtain the full tropospheric response. Thus, the wave driving most responsible for the tropospheric response to the final warming is in the lower stratosphere and upper troposphere (50–500 hPa).

e. *Wave-1 evolution across the final warming*

The evolution of the anomalous zonal wind in the zonally symmetric model forced only by wave driving due to planetary wave 1 is similar to that in the full model (not shown), indicating that wave 1 is most important for the downward influence in our model. The composite wave-1 amplitude from the full model is shown in Fig. 13. A burst of wave-1 amplitude appears in the upper troposphere/lower stratosphere, between 70 and 500 hPa, while in the stratosphere the wave weakens, suggesting that the amplification of wavenumber 1 prior to the final warming is very important for the deceleration of the tropospheric zonal wind.

5. Summary and discussion

We obtained 80-member ensembles of the springtime transition by imposing a seasonal transition in the stratospheric radiative equilibrium temperature. Our results show that that the timing of the final warming depends on the radiative forcing and on the strength of the wave activity. A small radiative zonal wind forcing and strong planetary wave activity generally result in an early final warming, and vice versa. The zonal wind evolution computed from model composites shows that when the stratosphere undergoes the transition from wintertime to summertime, high-latitude tropospheric zonal winds decelerate as well. With stronger topographic forcing, the stratospheric transition becomes more abrupt, and the tropospheric changes become larger. Transitions with weak topographic forcings resemble the observations of final warmings in the SH (BM07b), while those with strong topographic forcing resemble the observations of final warmings in the NH (BMR06). In our model, since the radiatively driven seasonal transition occurs only in the stratosphere, these tropospheric signals must be initiated by the radiatively driven changes in the stratospheric circulation, suggesting that much of the observed tropospheric signal during final warmings is likewise initiated from the stratosphere.

We explore the mechanisms through which the stratospheric final warming exerts its downward influence on the tropospheric circulation. The comparison between anomalous longwave and shortwave E–P flux divergence in section 4b shows that planetary waves play an important role in causing the stratospheric and tropospheric deceleration prior to the final warming. The zonally symmetric model run with longwave forcing also confirms that the downward influence of the final warming involves interactions between long waves and the zonal-mean flow in high latitudes within the troposphere.

Without topography, previous studies indicated that tropospheric synoptic-eddy feedback is primarily responsible for the tropospheric responses to stratospheric wave driving (Kushner and Polvani 2004; SR04). Planetary waves are also important for communicating the stratospheric influence down into the troposphere, but their response, mostly due to wavenumber 3 in SR04's model, is much weaker than the synoptic eddies (SR04). This differs markedly from our results for final warmings in the presence of strong topography, in which the planetary waves are important and no synoptic-eddy feedback is evident. Possibly this relates to the decorrelation time of the annular model with and without topography. Gerber and Vallis (2007) showed that the intrinsic time scale of the annular mode is shorter in the presence of topography or some other stationary wave forcing. This

implies a weak transient-eddy feedback when the jet is not zonally symmetric. Gerber and Polvani (2009) also found that topography weakens the tropospheric response to stratospheric anomalies substantially. Chan and Plumb (2009) showed that the impact of the troposphere on stratospheric perturbations is quite sensitive to the state of the troposphere. More importantly, the responses of SR04 and Kushner and Polvani (2004) are in steady-state simulations, while the final warming is a transient event. As such, the final warming may not allow enough time for the synoptic eddies to respond, so that the mechanism of the tropospheric eddy feedback is much weaker.

In the stratosphere, the zonal wind deceleration prior to the final warming is mostly driven by the anomalous wave activity, with some cancellation from the effect of the residual circulation. In the troposphere, the planetary-wave driving is nearly the same magnitude as the acceleration due to the residual circulation. Their difference determines the tropospheric zonal wind deceleration. Zonally symmetric model runs reveal that, by inducing the residual circulation, most of the tropospheric anomalies come from the contribution of wave driving in the lower stratosphere and upper troposphere. Once again, this points to the important role of tropospheric planetary waves in inducing the residual circulation and causing the zonal wind deceleration in the troposphere.

Our investigation indicates two mechanisms for the downward influence for the stratospheric final warming on the tropospheric circulation. The stratospheric anomalous wave driving induces a residual circulation, and this has an impact on the tropospheric circulation, similar to results in Haynes et al. (1991) and Thompson et al. (2006). On the other hand, the stratosphere can affect the propagation of planetary wave from the troposphere, and this results in a burst of planetary wave-1 activity in the troposphere prior to the final warming. This wave burst can induce the residual circulation and finally cause the tropospheric zonal wind deceleration.

The mechanism for the amplification of wave 1 in the tropospheric during the final warming is not clear. Recent studies on the propagation of planetary waves—for example, wave reflection (Perlwitz and Harnik 2003, 2004), refraction (Simpson et al. 2009), trapping (BM07a), and resonance (Scott and Haynes 2002)—provide possible explanations.

Overall, the pattern of downward influence of the final warming we obtained with 2000-m topography resembles that in NH observations (BMR06). Diagnostic analyses of the downward influence reveals that the planetary wave driving in the lower stratosphere and upper troposphere are important in inducing the residual circulation and causing zonal wind deceleration in the troposphere. This suggests that the planetary waves are crucial for the observed downward influence of the final warming.

Acknowledgments. We thank Dr. Yucheng Song for the discussion on the model equation deduction. We also thank the reviewers for their insightful and helpful comments. LS and WR are supported by the National Science Foundation (NSF) climate and large-scale dynamical program under Grant ATMS-0456157. LS and GC are supported by a start-up fund provided by Cornell University.

APPENDIX A

Atmospheric Dynamical Model

In the dynamical model, radiative processes are parameterized by Newtonian cooling. The temperature is relaxed to a zonally symmetric equilibrium temperature field,

$$\frac{\partial T}{\partial t} = \cdots - \alpha(z)[T - T_{\mathrm{eq}}(\phi, z)], \qquad \text{(A1)}$$

where $\alpha(z) = 1/\tau(z)$ is the relaxation rate and $\tau(z)$ is the relaxation time. The relaxation rate is that used by Holton and Mass (1976). It is a function of height, given by $\alpha(z) = \{1.5 + \tanh[(z - 35\ \mathrm{km})/7\ \mathrm{km}]\} \times 10^{-6}\ \mathrm{s}^{-1}$, where z is the mean altitude of the model sigma level. The relaxation time $\tau(z)$ varies from about 23 days in the troposphere to about 4 days in the stratosphere.

The equilibrium temperature is a function of latitudes and pressure. In the troposphere, the equilibrium temperature is similar to Held and Suarez (1994), in which

$$T_{\mathrm{eq}} = \max\left\{T_{\mathrm{pt}}, \left[315\ \mathrm{K} - (\Delta T)_y \sin^2\phi - (\Delta\theta)_z \log\left(\frac{p}{p_0}\right)\cos^2\phi\right]\left(\frac{p}{p_0}\right)^{\kappa}\right\}, \qquad \text{(A2)}$$

where $T_{\mathrm{pt}} = 216.43$ K is the reference temperature at 100 hPa, $(\Delta T)_y = 60$ K, $(\Delta\theta)_z = 10$ K, and $\kappa = 2/7$. In the stratosphere, the equilibrium temperature is calculated from the radiative zonal winds, similar to Scott and Haynes (1998), using thermal wind relation. The midwinter (NH) and midsummer (SH) radiative zonal winds are

$$U_R(\phi, z) = \cos\phi \cos\left(\frac{\pi}{2}\frac{z - z_B}{z_U - z_B}\right)\{u_0 \tanh[b_0(\phi - \phi_0)] + J_1 + J_2 + J_3\} \qquad \text{(A3)}$$

for constant u_0, b_0, and ϕ_0, with $z_B = 11.4$ km and $z_U = 105$ km, and the $J_i(\phi, z)$ are defined as

$$J_i = u_i \operatorname{sech}[b_i(\phi - \phi_i)] \operatorname{sech}[a_i(z - z_i)], \quad i = 1, 2, 3 \tag{A4}$$

for constant u_i, b_i, ϕ_i, a_i, and z_i. The values of the constants for the velocity profile used in our calculation are

$$u_0 = 20 \text{ m s}^{-1}, \quad b_0 = 0.1, \quad \phi_0 = 20°, \tag{A5}$$

$$u_1 = 280 \text{ m s}^{-1}, \quad b_1 = 0.04, \quad \phi_1 = 60°, \quad a_1 = 0.05, \quad z_1 = 65 \text{ km}, \tag{A6}$$

$$u_2 = -20 \text{ m s}^{-1}, \quad b_2 = 0.1, \quad \phi_2 = 15°, \quad a_2 = 0.3, \quad z_2 = 30 \text{ km}, \tag{A7}$$

and

$$u_3 = -220 \text{ m s}^{-1}, \quad b_3 = 0.03, \quad \phi_3 = -55°, \quad a_3 = 0.04, \quad z_3 = 70 \text{ km}. \tag{A8}$$

Thus, the stratospheric radiative velocity can be regarded as a superposition of three jets, which we take to be a westerly midlatitude winter jet u_1, an easterly midlatitude summer jet u_3, and an easterly equatorial jet u_2. The stratospheric and tropospheric T_{eq} are separated at 100 hPa. Figure 1a shows the equilibrium temperature. The NH and SH are in the midwinter and midsummer, respectively. Figure 1b shows the climatological zonal wind in the perpetual run with fixed T_{eq} as in Fig. 1a and 2000-m wave-1 topographic forcing in the NH.

The topography is idealized and similar to that used by Taguchi et al. (2001), which is

$$h(\lambda, \phi) = \begin{cases} 4h_0\mu^2(1 - \mu^2)\sin(m\lambda), & \mu \geq 0 \\ 0, & \mu < 0, \end{cases} \tag{A9}$$

where $\mu = \sin(\phi)$ and m is the zonal wavenumber. Since NH final warming resembles the "vortex displacement" (Charlton and Polvani 2006) of the sudden warming, in which zonal wavenumber 1 is more important (Fig. 5 in BM07a), here, unless specified otherwise, we set m to 1, although we also provide a brief discussion of wavenumber-2 final warmings. The amplitude of the topographic forcing is represented by h_0. We test six different amplitudes from 500 to 3000 m every 500 m. For each h_0 value, 80 realizations of seasonal transitions have been carried out, and these are used to analyze the final warming events.

In the dynamical model, we follow SR04 to consider the near-surface drag $k(\sigma)\mathbf{v}$ for $\sigma > 0.8$, where $\mathbf{v}$ is the horizontal wind vector with components u and v. The damping coefficient is given by

$$k(\sigma) = \begin{cases} 0, & \sigma \leq 0.8 \\ \dfrac{1}{\tau}\dfrac{\sigma - 0.8}{0.2}, & \sigma > 0.8, \end{cases} \tag{A10}$$

where $\tau = 0.5$ day is the damping time scale. Vertical diffusions used in the momentum and thermodynamic equations are also the same as SR04.

APPENDIX B

Zonally Symmetric Model

The zonally symmetric model is derived from the full model and only zonal mean components of the vorticity, divergence, temperature, and the natural logarithm of the surface pressure are integrated every time step. In the zonally symmetric model, the eddy forcing in the y momentum equation can be neglected and we only consider the eddy forcing for the zonal wind, temperature, and logarithm surface pressure equations, represented by F_u, F_T, and $F_{\ln P_s}$, respectively.

The zonally symmetric model equations are

$$\frac{\partial \overline{u}}{\partial t} + \overline{v}\left[\frac{1}{a\cos\phi}\frac{\partial(\overline{u}\cos\phi)}{\partial\phi} - f\right] + \overline{\dot{\sigma}}\frac{\partial \overline{u}}{\partial\sigma} = F_u, \tag{B1}$$

$$\frac{\partial \overline{T}}{\partial t} + \frac{\overline{v}}{a}\frac{\partial \overline{T}}{\partial\phi} + \overline{\dot{\sigma}}\frac{\partial \overline{T}}{\partial\sigma} - \kappa\overline{T}\overline{\left(\frac{\omega}{p}\right)} = F_T, \tag{B2}$$

$$\frac{\partial \overline{\ln P_s}}{\partial t} + \frac{\overline{\tilde{v}}}{a}\frac{\partial \overline{\ln P_s}}{\partial\phi} + \overline{\tilde{D}} = F_{\ln P_s}, \tag{B3}$$

and

$$\frac{\partial \overline{\dot{\sigma}}}{\partial\sigma} + \frac{\overline{v} - \overline{\tilde{v}}}{a}\frac{\partial \overline{\ln P_s}}{\partial\phi} + (\overline{D} - \overline{\tilde{D}}) = 0, \tag{B4}$$

where the overbar and tildes represent zonal and vertical averages, respectively. The prime means the deviation from the zonal mean; a is the radius of the earth; f is the Coriolis parameter; R is the gas constant for dry air; κ is the ratio of gas constant to specific heating at constant pressure; u, v, D, T, and P_s are the zonal wind, meridional wind, divergence, temperature, and surface pressure, respectively; $\dot{\sigma}$ and ω are the vertical velocity in the sigma and pressure coordinates, respectively; p is the pressure associated with the

sigma level ($p = P_s\sigma$); and ϕ is the latitude. The eddy forcings are

$$F_u = \frac{1}{\overline{P_s}}\left\{-\frac{1}{a\cos^2\phi}\frac{\partial[\overline{(P_s v)'u'}\cos^2\phi]}{\partial\phi} - \frac{\partial\overline{(P_s\dot{\sigma})'u'}}{\partial\sigma} - \frac{1}{a\cos\phi}\overline{P_s'\frac{\partial(\Phi - RT)'}{\partial\lambda}} + C_u\right\}, \quad \text{(B5)}$$

$$F_T = \frac{1}{\overline{P_s}}\left\{-\frac{1}{a\cos\phi}\frac{\partial[\overline{(P_s v)'T'}\cos\phi]}{\partial\phi} - \frac{\partial\overline{(P_s\dot{\sigma})'T'}}{\partial\sigma} + C_{T1} + C_{T2}\right\}, \quad \text{(B6)}$$

and

$$F_{\ln P_s} = -\overline{\tilde{\mathbf{v}}'\cdot\nabla(\ln P_s)'}, \quad \text{(B7)}$$

where λ is the longitude, Φ is the geopotential height, and $\mathbf{v}$ is the horizontal wind vector with components u and v. The first three terms in Eq. (B5) are meridional momentum flux, vertical momentum flux, and form drag. The first two terms in Eq. (B6) are meridional heat flux and vertical heat flux; $F_{\ln P_s}$, C_u, C_{T1}, and C_{T2} are the corrections to the zonally symmetric model by considering the extra covariances in the full model:

$$C_u = -\overline{P_s'v'}\left[\frac{1}{a\cos\phi}\frac{\partial(\overline{u}\cos\phi)}{\partial\phi} - f\right] - (\overline{P_s'\dot{\sigma}'} + \overline{P_s}\delta\bar{\dot{\sigma}})\frac{\partial\overline{u}}{\partial\sigma}, \quad \text{(B8)}$$

$$C_{T_1} = -\frac{\overline{P_s'v'}}{a}\frac{\partial\overline{T}}{\partial\phi} - (\overline{P_s'\dot{\sigma}'} + \overline{P_s}\delta\bar{\dot{\sigma}})\frac{\partial\overline{T}}{\partial\sigma}, \quad \text{(B9)}$$

and

$$C_{T_2} = \kappa\left[\overline{P_s\left(\frac{\omega}{p}\right)T} - \overline{P_s}\,\overline{\left(\frac{\omega}{p}\right)}\,\overline{T}\right], \quad \text{(B10)}$$

where $\delta\bar{\dot{\sigma}}$ is the correction to the diagnosed sigma vertical velocity in the zonally symmetric model and can be obtained by

$$\frac{\partial(\delta\bar{\dot{\sigma}})}{\partial\sigma} = -\overline{(\mathbf{v} - \tilde{\mathbf{v}})'\cdot\nabla(\ln P_s)'}. \quad \text{(B11)}$$

In practice, before the zonally symmetric run F_u, F_T, and $F_{\ln P_s}$ are first diagnosed from the full model based on Eqs. (B5)–(B7), respectively. When running the zonally symmetric model, we transfer F_u, F_T, and $F_{\ln P_s}$ into spectral fields, then add the spectral eddy forcings to the vorticity, divergence, temperature, and logarithm surface pressure tendency terms every time step. The resulting evolution of zonal winds will be very similar to the full model.

REFERENCES

Andrews, D. G., J. R. Holton, and C. B. Leovy, 1987: *Middle Atmosphere Dynamics*. Academic Press, 489 pp.

Ayarzagüena, B., and E. Serrano, 2009: Monthly characterization of the tropospheric circulation over the Euro-Atlantic area in relation with the timing of stratospheric final warmings. *J. Climate,* **22,** 6313–6324; Corrigendum, **23,** 2232.

Black, R. X., 2002: Stratospheric forcing of surface climate in the Arctic Oscillation. *J. Climate,* **15,** 268–277.

——, and B. A. McDaniel, 2007a: The dynamics of Northern Hemisphere stratospheric final warming events. *J. Atmos. Sci.,* **64,** 2932–2946.

——, and ——, 2007b: Interannual variability in the Southern Hemisphere circulation organized by stratospheric final warming events. *J. Atmos. Sci.,* **64,** 2968–2974.

——, ——, and W. A. Robinson, 2006: Stratosphere–troposphere coupling during spring onset. *J. Climate,* **19,** 4891–4901.

Chan, C. J., and R. A. Plumb, 2009: The response to stratospheric forcing and its dependence on the state of the troposphere. *J. Atmos. Sci.,* **66,** 2107–2115.

Charlton, A. J., and L. M. Polvani, 2006: A new look at stratospheric sudden warmings. Part I: Climatology and modeling benchmarks. *J. Climate,* **20,** 449–469.

Chen, G., and I. M. Held, 2007: Phase speed spectra and the recent poleward shift of Southern Hemisphere surface westerlies. *Geophys. Res. Lett.,* **34,** L21805, doi:10.1029/2007GL031200.

——, and P. Zurita-Gotor, 2008: The tropospheric jet response to prescribed zonal forcing in an idealized atmospheric model. *J. Atmos. Sci.,* **65,** 2254–2271.

Chen, P., and W. A. Robinson, 1992: Propagation of planetary waves between the troposphere and stratosphere. *J. Atmos. Sci.,* **49,** 2533–2545.

Farrara, J. D., and C. R. Mechoso, 1986: An observational study of the final warming in the Southern Hemisphere stratosphere. *Geophys. Res. Lett.,* **13,** 1232–1235.

Gerber, E. P., and G. K. Vallis, 2007: Eddy–zonal flow interactions and the persistence of the zonal index. *J. Atmos. Sci.,* **64,** 3296–3311.

——, and L. M. Polvani, 2009: Stratosphere–troposphere coupling in a relatively simple AGCM: The importance of stratospheric variability. *J. Climate,* **22,** 1920–1933.

Gordon, C. T., and W. F. Stern, 1982: A description of the GFDL global spectral model. *Mon. Wea. Rev.,* **110,** 625–644.

Haynes, P. H., M. E. McIntyre, T. G. Shepherd, C. J. Marks, and K. P. Shine, 1991: On the ''downward control'' of extratropical diabatic circulations by eddy-induced mean zonal forces. *J. Atmos. Sci.,* **48,** 651–678.

Held, I. M., and M. J. Suarez, 1994: A proposal for the intercomparison of the dynamical cores of atmospheric general circulation models. *Bull. Amer. Meteor. Soc.,* **75,** 1825–1830.

Holton, J. R., and C. Mass, 1976: Stratospheric vacillation cycle. *J. Atmos. Sci.,* **33,** 2218–2225.

Kushner, P. J., and L. M. Polvani, 2004: Stratosphere–troposphere coupling in a relatively simple AGCM: The role of eddies. *J. Climate,* **17,** 629–639.

Perlwitz, J., and N. Harnik, 2003: Observational evidence of a stratospheric influence on the troposphere by planetary wave reflection. *J. Climate,* **16,** 3011–3026.

——, and ——, 2004: Downward coupling between the stratosphere and troposphere: The relative roles of wave and zonal mean processes. *J. Climate,* **17,** 4902–4909.

Robinson, W. A., 1994: Eddy feedbacks on the zonal index and eddy-zonal flow interactions induced by zonal flow transience. *J. Atmos. Sci.,* **51,** 2553–2562.

——, 1996: Does eddy feedback sustain variability in the zonal index? *J. Atmos. Sci.,* **53,** 3556–3569.

——, 2000: A baroclinic mechanism for the eddy feedback on the zonal index. *J. Atmos. Sci.,* **57,** 415–422.

Salby, M. L., and P. F. Callaghan, 2007: Influence of planetary wave activity on the stratospheric final warming and spring ozone. *J. Geophys. Res.,* **112,** D20111, doi:10.1029/2006JD007536.

Scinocca, J. F., and P. H. Haynes, 1998: Dynamical forcing of stratospheric planetary waves by tropospheric baroclinic eddies. *J. Atmos. Sci.,* **55,** 2361–2392.

Scott, R. K., and P. H. Haynes, 1998: Internal interannual variability of the extratropical stratospheric circulation: The low-latitude flywheel. *Quart. J. Roy. Meteor. Soc.,* **124,** 2149–2173.

——, and ——, 2002: The seasonal cycle of planetary waves in the winter stratosphere. *J. Atmos. Sci.,* **59,** 803–822.

Simpson, I. R., M. Blackburn, and J. D. Haigh, 2009: The role of eddies in driving the tropospheric response to stratospheric heating perturbations. *J. Atmos. Sci.,* **66,** 1347–1365.

Song, Y., and W. A. Robinson, 2004: Dynamical mechanisms for stratospheric influences on the troposphere. *J. Atmos. Sci.,* **61,** 1711–1725.

Sun, L., 2010: Downward influence of stratospheric final warming events in an idealized model. Ph.D. thesis, University of Illinois at Urbana–Champaign, 133 pp.

——, and W. A. Robinson, 2009: Downward influence of stratospheric final warming events in an idealized model. *Geophys. Res. Lett.,* **36,** L03819, doi:10.1029/2008GL036624.

Taguchi, M., T. Yamaga, and S. Yoden, 2001: Internal variability of the troposphere–stratosphere coupled system simulated in a simple global circulation model. *J. Atmos. Sci.,* **58,** 3184–3203.

Thompson, D. W. J., J. C. Furtado, and T. G. Shepherd, 2006: On the tropospheric response to anomalous stratospheric wave drag and radiative heating. *J. Atmos. Sci.,* **63,** 2616–2629.

Waugh, D. W., and P. Rong, 2002: Interanual variability in the decay of lower stratospheric arctic vortices. *J. Meteor. Soc. Japan,* **80,** 997–1012.